

IMPROVED 3-D GPR DETECTION BY NUFFT COMBINED WITH MPD METHOD

Y.-Q. Huang, Y.-H. Liu, Q. H. Liu, and J.-Z. Zhang[†]

School of Information Science and Technology
Xiamen University
Xiamen, Fujian 361005, China

Abstract—A combined method of the non-uniform fast fourier transform (NUFFT) migration and the least-square based matching pursuit decomposition (MPD) algorithms is proposed to obtain better discrimination and interpretation for subsurface from ground penetrating radar (GPR) signals. By using the modified NUFFT migration algorithm, a fast and high resolution GPR reconstruction can be obtained with an additional reduction in storage and computation requirements. By incorporating the MPD algorithm into a migration method, denoised reconstructions are obtained to enhance objects detection, including the identification of objects' geometries and the estimation of their sizes and locations. Several examples from synthetic data and field data are demonstrated to establish the effectiveness of the synergic effect by comparing it with the conventional migration methods.

1. INTRODUCTION

GPR is a geophysical exploration technique with high efficiency, non-destructiveness and high resolution. To date, its application has spread to various engineering fields, including landmine detection, pavement and tunnel detection, groundwater contamination analysis, and underground archeology, *etc.* [1–4]. Generally, these applications can be classified as a problem of target detection and discrimination.

A widely used approach for target detection is image reconstruction from GPR data through a migration algorithm. The phase migration method, which is also called frequency-wavenumber (F-K) mi-

Corresponding author: J.-Z. Zhang (zhangjz@xmu.edu.cn).

[†] All the authors are also with Department of Electrical and Computer Engineering, Duke University, Durham, NC 27708, USA.

gration method, is of great interest in recent years [5–7]. An integral transform of target function spectrum $S(k_x, k_y, \omega)$ in the F-K domain is the key step of the phase migration implementation. The reconstructed target image is described as

$$I(x, y, z) = \frac{1}{8\pi^3} \int S(k_x, k_y, \omega) e^{j(k_x x + k_y y + k_z z)} dk_x dk_y d\omega \quad (1)$$

where $S(k_x, k_y, \omega)$ is the Fourier transform of the recorded GPR signal $s(x, y, t)$ at the air-ground interface ($z = 0$) plane; k_x, k_y, k_z, ω are the corresponding wavenumbers and angular frequency in the F-K domain samples. The F-K domain samples are governed by the GPR spatial frequency mapping function,

$$k_z = \sqrt{4(\omega/v)^2 - k_x^2 - k_y^2} \quad (2)$$

where v is the EM wave propagation speed in the subsurface medium. Due to a uniform planar scan and time interval, equally sampling points are normally used in k_x, k_y , and ω space, so that k_z samples calculated by Equation (2) are unevenly spaced. Thus, the problem stated in Equation (1) is usually discretized and then numerically evaluated by interpolation methods (such as linear interpolation and stolt interpolation [8–10]) followed by the uniform fast Fourier transform (FFT). Recently, Song et al. applied the NUFFT algorithm [11, 12] to directly solve Equation (1) and effectively obtain reconstructions for GPR imaging [6, 7]. Later, Liu et al. developed a modified NUFFT method [13] by using real interpolation coefficients to reduce the storage and computational cost. In this paper, we adopt the modified NUFFT algorithm in [13] to achieve the phase migration reconstructions of GPR data.

However, when a GPR system is used to probe deep objects (or when the soil is seriously lossy), EM waves will suffer from amplitude attenuation and noise interference leading to poor image reconstruction and target discrimination by using the phase migration method. Recently, spectral decomposition methods based on continuous wavelet transform (CWT), according to seismic discontinuity mapping, have been proven potentially valuable for GPR signal interpretation [14, 15]. One of the most popular and widely used spectral decomposition method is called the matching pursuit decomposition (MPD). For efficient computation, Liu and Marfurt developed the MPD method with the least-square concept, then decomposed each seismic waveform into a linear summation of wavelets and analyzed the spectrum [16]. These developments of the MPD method with its application to GPR signal processing were based on raw data sets received and the analytically interpretations were carried out in the time-frequency

domain. Therefore, it is still unknown for us how the synergic effect of the NUFFT and the MPD algorithms would perform for the object detection from weak and noisy GPR signals.

In this work, we combine the NUFFT method and the least-square based MPD approach and find the proposed technique plays an important role in denoising. Several synthetic and field data tests are provided and compared with the conventional interpolation FFT migration method to show the synergic effect of the NUFFT and the MPD algorithms, including the improvement of the signal-noise ratio (SNR), and the estimation of target's geometry and location.

2. ALGORITHM METHODOLOGY

2.1. The Modified NUFFT Migration Algorithm

The discretized form of the triple integral solution in the phase migration method in Equation (1) is given by

$$I(x_p, y_q, z_r) = \zeta \sum_{l=0}^{L-1} \sum_{m=0}^{M-1} \sum_{n=0}^{N-1} S(k_x^l, k_y^m, \omega^n) e^{j(k_x^l x_p + k_y^m y_q + k_z^n z_r)} \quad (3)$$

where $\zeta = \frac{\Delta k_x \Delta k_y \Delta \omega}{8\pi^3}$, Δk_x , Δk_y , $\Delta \omega$ are sampling steps in the F-K domain, L , M , N are total GPR sampling numbers in x , y and t directions, respectively, and x_p , y_q and z_r are sampling points of physical positions for 3-D reconstruction image coverage ($0 \leq p \leq L - 1$; $0 \leq q \leq M - 1$; $0 \leq r \leq N - 1$).

In the above expression, the two summations with respect to k_x and k_y space can be implemented by the FFT algorithm,

$$\begin{aligned} S'(x_p, y_q, \omega^n) &= \xi \sum_{l=0}^{L-1} \sum_{m=0}^{M-1} S(k_x^l, k_y^m, \omega^n) e^{j(k_x^l x_p + k_y^m y_q)} \\ &= FFT_{k_x} \left\{ FFT_{k_y} \left\{ S(k_x^l, k_y^m, \omega^n) \right\} \right\} \end{aligned} \quad (4)$$

where $\xi = \frac{\Delta k_x \Delta k_y}{4\pi^2}$. Then, the remaining computation for the third summation becomes

$$I(x_p, y_q, z_r) = \sum_{n=0}^{N-1} S'(x_p, y_q, \omega^n) e^{jk_z^n z_r} \quad (5)$$

Equation (5) can be realized by the 1st type NUFFT (NUFFT-1). Since Liu et al. recently proved that the least-square kernels in NUFFT algorithm are real-valued if conjugate-symmetric scaling factors are used [13], here we summarize the modified NUFFT-1 algorithm with

a same scaling factors treatment to reduce storage and computational cost for GPR imaging. For more details on modified 2nd type NUFFT (NUFFT-2), readers are referred to [13].

Below we use the shortened form I_r to substitute for $I(x_p, y_q, z_r)$. Then Equation (5) can be written as

$$I_r = \sum_{n=0}^{N-1} S_n'' e^{ic_n(r-N/2)\frac{2\pi}{N}} \quad (6)$$

where $S_n'' = S'(x_p, y_q, \omega^n) e^{ic_n\pi}$ and $c_n = k_z^n v \frac{N\Delta t}{2\pi}$. Then the NUFFT-1 algorithm for calculating Equation (6) is listed as following:

- 1) Precompute the inverse of *regular Fourier matrix* \mathbf{F}^{-1} [11] and cosine scaling factors $s_r^{-1} = \sec(\frac{\pi(r-N/2)}{\mu N})$ for later use.
- 2) Calculate least-square NUFFT kernels $\Phi_l(c_n)$ [11] with complexity of $O(N(q+1)^2)$. Here, $l = 0, \dots, q$.
- 3) Find a new set of Fourier coefficients by real-valued kernel convolution

$$\alpha_k = \sum_{n,l, [\mu c_n] + l = k} S_n'' \text{Re}[\Phi_l(c_n)] \quad (7)$$

with complexity of $O(N(q+1))$. $2N(q+1)$ multiplications and $N(q+1)$ storage units are saved by the treatment of ignoring the imaginary part of each kernel.

- 4) Carry out uniform FFT to evaluate

$$T_r = \sum_{p=-\mu N/2}^{\mu N/2-1} \alpha_p e^{i2\pi p(r-N/2)/\mu N}.$$

The complexity is $O(\mu N \log N)$.

- 5) Scale the values to obtain solutions by $\tilde{I}_r = T_r \cdot s_r^{-1}$ with least-square error. The complexity is $O(N)$.

It is also worth noting that only the real part of GPR image reconstruction result generated by the modified NUFFT migration method is used for later analysis and interpretation in this work. Thus, we can realize step 5) in the modified-NUFFT algorithm by $\tilde{I}_r = \text{Re}[T_r] \cdot s_r^{-1}$. This modification halves the storage and computational requirements for the scaling step. It is obvious that for $L \times M$ GPR scans on the xy plane, a total reduction of $2LMN(q+2)$ multiplications is obtained.

In this work, we consider the storage size at the moment, when requires a maximum storage space among the NUFFT steps,

and the MPD algorithm introduced below, as the lowest storage requirement for hardware. Then, it is easy to find that the minimum storage requirement, which depends on the step of Fourier coefficients calculation in the NUFFT method, should be reduced from $2LMN(q+3)$ to $LMN(q+5)$. For high accuracy, we usually choose the kernel size $q \geq 8$. Thus, more than 40% the storage space can be saved. This is a significant improvement as hardware sometimes has constraints on memory, especially when the scanning time is long and the planar scan is density with a big coverage.

2.2. Least-square Based MPD Method and Multi-spectral Attributes

In this part, we aim to enhance target detection from a poor migration image. Since the matching pursuit decomposition (MPD) method has been proven valuable in seismic exploration and production, we apply this technique to the modified NUFFT GPR image reconstruction to obtain a better interpretation of GPR signals.

The work [17] on GPR spectrum analysis gives evidence that Ricker wavelets provide a good representation for many commercial GPR signals. Therefore, we assume that each image profile at each observer location (x_p, y_q) , can be represented by a linear summation of individual Ricker wavelets, given by

$$I_r(x_p, y_q, z) = I_r(x_p, y_q, vt) = \sum_j a_j R(t - t_j, f_j, \varphi_j) + \text{Noise} \quad (8)$$

where a_j , t_j , f_j and φ_j are peak amplitude, center time (also called time delay), peak frequency and phase for each selected wavelet, respectively. R represents Ricker wavelets.

The greedy procedure of each time selecting an optimal wavelet, from an over-complete set of wavelet dictionary, leads to its main drawback of huge computational cost. To speed up its computation, Liu and Marfurt (2005) utilized analytic signals and incorporated the least-square error concept into the MPD method [16]. Thus the amplitude a_j and phase φ_j for each wavelet can be obtained as a closed-form solution. Let \mathbf{A}_j represents the complex amplitude equal to $a_j e^{i\varphi_j}$, then its closed-form solution in a matrix form is,

$$\mathbf{A} = [\mathbf{R}^H \mathbf{R} + \varepsilon \mathbf{U}]^{-1} \mathbf{R}^H \mathbf{I} \quad (9)$$

where \mathbf{I} represents the analytic image reconstruction signal, \mathbf{R} indicates analytic Ricker wavelets, ε is a small adjustment coefficient which makes the solution stable and \mathbf{U} is an identity matrix. Thus,

the analytic analogue of Equation (8) is,

$$\mathbf{I}(x_p, y_q, z) = \mathbf{I}(x_p, y_q, vt) = \sum_j \mathbf{A}_j \mathbf{R}(t - t_j, f_j) + \text{Noise} \quad (10)$$

Then, the least-square based MPD is proceeded in a loop: 1) read real-valued GPR image as the input, set residual equal to $I_r(t)$ and give a desired threshold; 2) fix t_j by picking the time position of the peak of the input envelope, calculate f_j by estimating the average frequency of the wavelet and find least-square solution to complex amplitude; 3) calculate the residual by subtracting the computed complex wavelet to form a new residual; 4) go to step 2) if the residual energy is larger than the threshold value, or stop.

According to the efficient MPD algorithm introduced above, we make use of the useful information which each wavelet provides and define the denoised signal as,

$$\mathbf{I}_d(x_p, y_q, z) = \sum_j \mathbf{A}_j \mathbf{R}(t - t_j, f_j) \quad (11)$$

The instantaneous power and phase spectra can be simply obtained from the analytic signal calculated by Equation (11). The instantaneous power spectrum is proportional to the reflectivity distribution and gives a direct response to reflection strength at every moment. Since the noise can be mostly removed through incorporating the MPD method into the NUFFT reconstruction, the estimation accuracy of target's geometry, size and location can be improved, aside from an enhancement of SNR. Besides, the instantaneous phase is considered to measure the continuity of the phase variation. With a significant property that instantaneous phase is independent of reflection strength, it is helpful for weak reflections detection.

3. NUMERICAL RESULTS

Several tests from synthetic data and field data are demonstrated as follows. It is noted that the linear interpolation FFT algorithm is employed as a conventional phase migration method for comparison. For the modified NUFFT migration implementation, we use the over sampling rate $\mu = 2$ and the kernel size $q = 8$. In particular, for fair comparison, an isovalue equals to -3 dB relative to the maximum is used in all tests for targets' discrimination and estimation.

3.1. Test from Synthetic Data

The synthetic data are generated by the Wavenology, a commercial software package developed by Wave Computation Technologies Inc.

(WCT). A target of “D” shape symbol ($\epsilon_r = 2$) located in a free space is 32 cm high, 16 cm wide, and 2 cm thick. 31×31 receivers are located 10 cm above the “D” target, with a uniform and planar scan interval of 2 cm. The excitation used is in the frequency range of 0.15–15 GHz with a uniformly time interval of 0.0031 ns.

In this case, the synthetic data is considered ideal and noise-free. Besides, since the conventional interpolation FFT method and the modified NUFFT method are different means to approximate the DFT format of the phase migration equation, it is reasonable to regard the DFT migration result of the noise-free synthetic data as a reference to measure the L_2 norm error. To simulate a noised data set for comparison, we manually add the white gaussian random

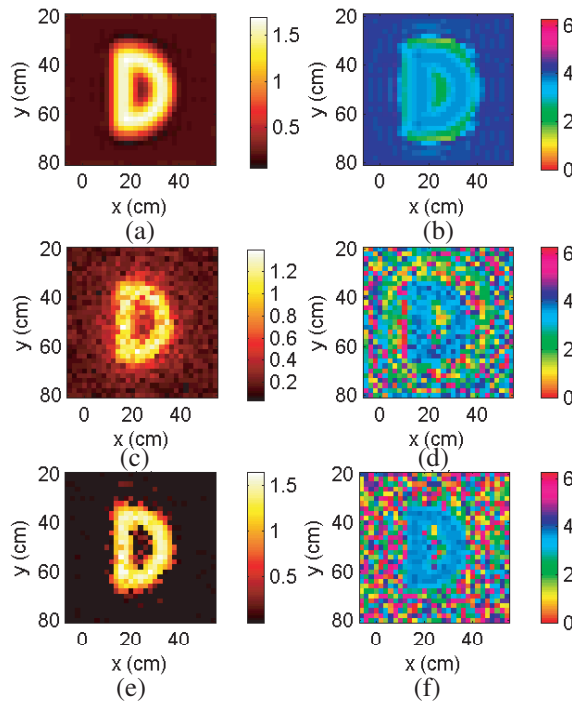


Figure 1. Instantaneous spectral distribution slice at $t = 0.79$ ns. Left and right columns show instantaneous power and phase spectra, respectively (same in the following Figs. 2–4). (a) and (b) are obtained by the DFT migration with noise-free data. (c) and (d) are obtained by the interpolation FFT migration with noisy data. (e) and (f) are obtained by our method with noisy data.

noise (WGRN) gradually before doing data processing. Suppose that it is acceptable if the L_2 norm error e_2 satisfies $e_2 \leq 30\%$, the noise tolerance can be improved from 5 dB for conventional interpolation FFT method to 10 dB for the proposed NUFFT-MPD method. It is also noted that the direct arrival of the synthetic signal is removed before processing.

The slice comparison of the instantaneous spectra distribution (power and phase) is provided in Fig. 1. Figs. 1(a) and (b) show the instantaneous spectra for a DFT reconstruction slice from the noise-free synthetic data; (c) and (d) are the instantaneous spectra slices from the noisy synthetic data with 10 dB WGRN, by the interpolation FFT migration method; (e) and (f) are the results obtained from the same noise data set, by the proposed combination method. One can see from (a) and (b) that the DFT migration result gives a good reconstruction image from noise-free GPR data, though the weak ‘‘Gibbs’’ ringing effect coming from the numerical error of Fourier transform is observed (ringing phenomena around the edge of ‘‘D’’) in the spectra distribution. The visualization in (c) and (d) can hardly give a good geometry of the targets as the edge is not sharp and the value inside the target is not continuous. Compared with the interpolation FFT result, the instantaneous spectra as shown in (e) and (f) indicate that the proposed NUFFT-MPD method gives a better discrimination of the target. A more detailed quantitative comparison, in terms of L_2 error, thickness estimation and the SNR, is summarized in Table 1. One can observe the better performance of the proposed method for both the noise-free and noisy cases.

Table 1. Comparison of relative error, thickness estimation and image SNR for noise-free and noisy synthetic data sets, respectively.

		DFT	Intrpl. FFT	NUFFT	NUFFT-MPD
Without Noise	L2 Error	-	5.47%	0.0007%	-
	Thickness Estimation (Value (cm)/Error)	1.72/ 13.98%	1.63/ 18.63%	1.72/ 13.98%	1.91/ 4.67%
	SNR (dB)	47.89	47.25	47.89	56.51
	L2 Error	51.38%	53.15%	51.32%	29.91%
With Noise	Thickness Estimation (Value (cm)/Error)	1.63/ 18.63%	1.58/ 20.95%	1.63/ 18.63%	1.81/ 9.33%
	SNR (dB)	41.93	41.5	41.82	52.04
	L2 Error	51.38%	53.15%	51.32%	29.91%

3.2. Test from Field Data

Following tests are done for available field data provided by Georgia Institute of Technology (reported in [6]).

In the first example, GPR data are collected in free space. 91×91 traces are scanned on the xy plane with a scanning step of 0.02 m. The GPR system works within the frequency band of 0.06 GHz–8.06 GHz. The recorded data was oversampled with a time interval of 0.018 ns (according to Nyquist sampling theory, the minimum sampling period should be 0.028 ns). The plywood sheet of the letters “GT” is 38.5 cm wide, 46.5 cm high, and 1.8 cm thick. Slice comparison of the instantaneous spectral distribution is shown in Fig. 2. Figs. 2(a) and (b) show instantaneous power and phase spectrum for the DFT migration result, respectively. Figs. 2(c) and (d) are the interpolation FFT results, while (e) and (f) are results by the proposed method.

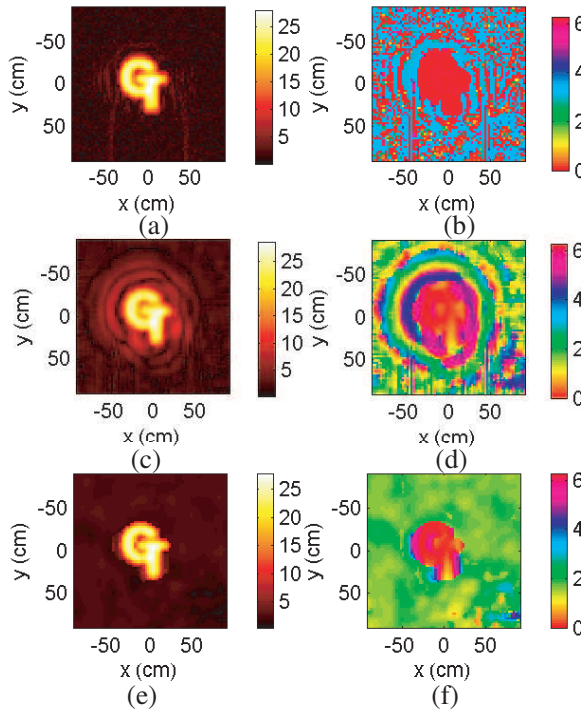


Figure 2. Instantaneous spectral distribution slice at $t = 7$ ns. (a) and (b) are obtained by the DFT migration. (c) and (d) are obtained by the interpolation FFT migration. (e) and (f) are obtained by our method.

One observes that the power spectra with different methods achieve good reconstructions for the plywood sheet consisting of “G” and “T” symbols, except that the power spectrum from the interpolation FFT result introduces some obvious “Gibbs” and background noise. However, from the comparison of phase spectra, one can find that the unwanted noise and artifacts are mostly removed by using the proposed method. One reason is that the instantaneous phase is sensitive to the discontinuity of phase variation, so weak variance that is not obvious enough in power spectrum can be detected. It also indicates that the instantaneous phase spectrum can give extra useful details of migration signals and achieve denoising performance for better interpretation. The numerical comparison of the thickness estimation and image SNR for well-sampled and undersampled cases is listed in Table 2. The improvement by the synergic effect of the proposed combination method is further confirmed. Besides, it is noticed that the synergic effect has the potential to sustain the performance of the DFT method on relatively sparse acquisitions. Thus, it is helpful to reduce acquisition time and save cost in practice.

In the second example we make use of GPR data reflected from a chamber of 20.32 cm thick and buried 9.5 cm deep in sand. The multi-static GPR operated in the similar way as in the first example. The true geometry of the chamber slice should be a rectangle. Fig. 3 shows the instantaneous spectral distribution slices of power and phase by the interpolation FFT method and the proposed approach, respectively. From the comparison of instantaneous power spectra, it is obvious that the proposed method plays a role of denoising and thus obtains a better

Table 2. Comparison of thickness estimation and image SNR for well-sampled and under-sampled cases in the first field example.

		DFT	Intrpl. FFT	NUFFT	NUFFT-MPD
Well-sampled	Thickness Estimation (Value (cm)/ Error)	1.65/ 8.33%	1.58/ 12.22%	1.65/ 8.33%	1.92/ 6.81%
	SNR (dB)	80.85	79.7	80.85	82.38
Under-sampled	Thickness Estimation (Value (cm)/ Error)	1.59/ 11.67%	1.51/ 16.11%	1.59/ 11.67%	1.65/ 8.33%
	SNR (dB)	72.25	70.42	72.16	81.24

image reconstruction without much background noise. The estimated dimensions of the buried chamber are listed in Table 3 and numerical comparison is also given associated with different methods. We observe an improvement of estimation accuracy and an enhancement of the SNR by our proposed method.

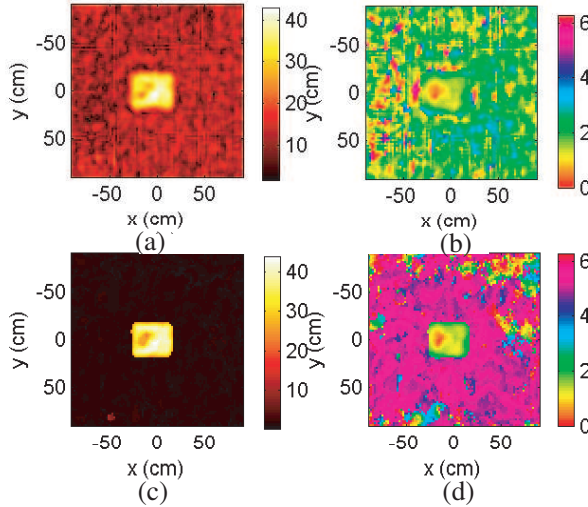


Figure 3. Instantaneous spectral distribution slice at $t = 5.31$ ns. (a) and (b) are obtained by the interpolation FFT migration. (c) and (d) are obtained by our method.

Table 3. Comparison of thickness estimation, depth estimation and image SNR for buried chamber in the second field example.

	DFT	Intrpl. FFT	NUFFT	NUFFT-MPD
Thickness Estimation (Value (cm)/ Error)	16.1/ 20.77%	15.9/ 21.75%	16.1/ 20.77%	17.1/ 15.85%
Depth Estimation (Value (cm)/ Error)	10.5 10.53%	10.5 10.53%	10.5 10.53%	9.9 4.04%
SNR (dB)	35.61	35.22	35.	40.05

The third example with several landmines and rock clutters buried in sand, is presented for further illustration of advantages with the data processing technique we proposed. All objects have different geometry sizes and are buried at different depths. Since the modified NUFFT method has already been verified superior to the interpolation FFT method, we compare the detection results of the proposed method with the modified NUFFT method (as shown in Fig. 4), rather than the interpolation FFT method. There are four objects in this depth slice. Three of them are in spherical shape and one is in cuboid shape. From the comparison of power distribution, again we observe the advantage of denoising with the proposed NUFFT-MPD method. However, it is hard to tell whether there is an object at the bottom right area because the power is very small. From the phase spectral image shown in Fig. 4(b), we can gain little further information for targets detection. However, a comprehensive explanation of spectra in Figs. 4(c) and (d) can provide a better discrimination for the four objects with geometries much closer to their ground truth. The numerical comparison is provided in Table 4. In this table, the objects are listed in a sequence first from the left to the right and then from the top to the bottom. Aside from an improvement of estimation accuracy, it is also noted that the geometries of the TMA-5 and the nylon cylinder can be recovered by our proposed method.

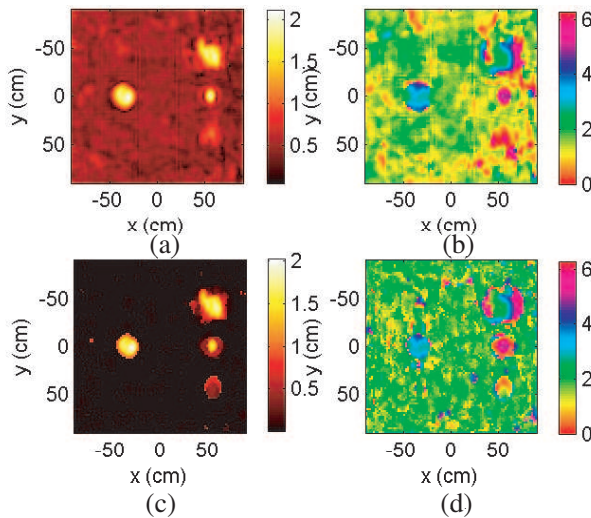


Figure 4. Instantaneous spectral distribution slice at $t = 0.15$ ns. (a) and (b) are obtained by the NUFFT migration. (c) and (d) are obtained by our method.

Table 4. Comparison of size estimation and image SNR for buried landmines in the third field example.

Object	Ground Truth (cm)			NUFFT	NUFFT-MPD
	Diameter	Length	Width	Estimation (cm) /Error	Estimation (cm) /Error
VS-1.6	22.6	-	-	26/2.58%	24/1.06%
TMA-5	-	30	27.5	Incorrect Geometry	39/30% 36/39%
VS-2.2	23	-	-	10/56.5%	26/13.04%
Nylon Cylinder	15.5	-	-	Incorrect Geometry	22/41.94%

4. CONCLUSION

This work incorporates the efficient least-square based MPD algorithm into the modified NUFFT migration method and presents a synergic effect for better GPR discrimination and detection. The modified NUFFT migration method has lower storage and CPU time requirement than the original NUFFT migration algorithm. By combining the fast MPD approach with the modified NUFFT migration method, most noise and artifacts can be removed and thus a better image is obtained. The synergic effect of the combination scheme has been observed from several theoretical and experimental tests. Since real GPR recorded data is rarely dominated by simple reflections from targets, the signal processing procedure we proposed is more useful for realistic applications.

ACKNOWLEDGMENT

Yueqin Huang and Jianzhong Zhang were supported in part by the National Science Foundation of China (No. 40774065), and in part by the Joint Ph.D. Fellowship Program of the China Scholarship Council. Experimental data sets were gracefully provided by Prof. Waymond Scott to Qing H. Liu in their joint publication in [6].

REFERENCES

1. Peters, L. P., J. Daniels, and J. J. Young, "Ground penetrating radar as a subsurface environmental sensing tool," *IEEE Proc.*, Vol. 82, 1802–1822, 1994.

2. Groenenboom, J. and A. Yarovoy, "Data processing and imaging in GPR system dedicated for landmine detection," *Subsurface Sensing Technologies and Appl.*, Vol. 3, No. 4, 387–402, 2002.
3. Danielsa, J. J., R. Roberts, and M. Vendlb, "Ground penetrating radar for the detection of liquid contaminants," *Appl. Geophys.*, Vol. 33, 195–207, 1995.
4. Fiorani, L., M. Bortone, S. Mattei, C. Ruocchio, S. Vetrella, and A. Salom, "Geoscope and Geolidar: Integrated instruments for underground archaeological investigations," *Subsurface Sensing Technologies and Appl.*, Vol. 1, No. 3, 305–319, 2000.
5. Gu, K., G. Wang, and J. Li, "Migration based SAR imaging for ground penetrating radar systems," *IEE Proc. Radar, Sonar, Navigation*, Vol. 151, 317–325, 2004.
6. Song, J., Q. H. Liu, K. Kim, and W. R. Scott, "High-resolution 3-D radar imaging through nonuniform fast Fourier transform (NUFFT)," *Commun. in Computat. Phys.*, Vol. 1, No. 1, 176–191, 2006.
7. Song, J., Q. H. Liu, P. Torriero, and L. Collins, "Two-dimensional and three-dimensional NUFFT migration method for landmine detection using ground-penetrating radar," *IEEE Trans. Geosci. Remote Sensing*, Vol. 44, 1462–1469, 2006.
8. Cafforio, C., C. Prati, and F. Rocca, "SAR data focusing using seismic migration techniques," *IEEE Trans. on Aerospace and Electronic Systems*, Vol. 27, 194–207, 1991.
9. Stolt, R. H., "Migration by Fourier transform," *Geophys.*, Vol. 43, No. 1, 23–48, 1978.
10. Li, A., "Algorithms for the implementation of Stolt interpolation in SAR processing," *Intl. Conf. Geosci. Remote Sensing Symp.*, 360–362, 1992.
11. Liu, Q. H. and N. Nguyen, "An accurate algorithm for nonuniform fast Fourier transform (NUFFT's)," *IEEE Trans. Microwave and Guided Wave Lett.*, Vol. 8, No. 1, 18–20, 1998.
12. Nguyen, N. and Q. H. Liu, "The regular Fourier matrices and nonuniform fast Fourier transforms," *SIAM J. Sci. Comput.*, Vol. 21, No. 1, 283–293, 1999.
13. Liu, Y.-H. and Q. H. Liu, "A new efficient FDTD time-to-frequency-domain conversion algorithm," *Progress In Electromagnetic Research*, PIER 92, 33–46, 2009.
14. Wang, Y., "Seismic time-frequency spectral decomposition by matching pursuit," *Geophys.*, Vol. 72, No. 1, 13–20, 2007.
15. Chakraborty, A. and D. Okaya, "Frequency-time decomposition

- of seismic data using wavelet-based methods,” *Geophys.*, Vol. 60, No. 6, 1906–1916, 1995.
16. Liu, J. and K. J. Marfurt, “Instantaneous spectral attributes to detect channels,” *Geophys.*, Vol. 72, No. 2, 23–31, 2007.
 17. Bradford, J. H. and Y. Wu, “Instantaneous spectral analysis: Time-frequency mapping via wavelet matching with application to contaminated-site characterization by 3D GPR,” *Leading Edge*, Vol. 26, No. 8, 1018–1023, 2007.